New Insight into Photoalignment of Liquid Crystals on Coumarin-Containing Polymer Films

Chunki Kim,[†,§] Anita Trajkovska,[†,§] Jason U. Wallace,[†,§] and Shaw H. Chen*[,†,‡]

Department of Chemical Engineering and Laboratory for Laser Energetics, University of Rochester, 240 East River Road, Rochester, New York 14623-1212

Received February 3, 2006; Revised Manuscript Received March 23, 2006

ABSTRACT: Polymers containing 6- and 7-substituted coumarin moieties were prepared as photoalignment films through linearly polarized UV irradiation to a varying fluence for an investigation of liquid crystal orientation. Model coumarin monomers and dimers were also synthesized and characterized as part of a novel approach to the interpretation of liquid crystal orientation in terms of monomer conversion. The experimental results for monomer conversion as a function of fluence were used to validate the first-order kinetics with an exponentially decaying rate constant as the reaction proceeds. A kinetic model was constructed to describe the evolutions of the orientational order on the parts of the reacted and the unreacted coumarin moieties. The model was instrumental to the visualization of liquid crystal orientation on photoalignment films at the early and the late stages of dimerization. Furthermore, the observed crossover in liquid crystal orientation on the polymer film comprising 7-substituted coumarin moieties was successfully interpreted by considering three factors: the relative abundance of the reacted and the unreacted coumarin moieties, the degrees of their orientational order predicted by the kinetic model, and the energetics of molecular interaction.

Introduction

A uniaxial orientation of liquid crystals is the foundation of a wide variety of electrooptic devices. Mechanical rubbing of a polyimide film has been widely practiced for its simplicity, but the dust, electrostatic charges, and mechanical damage resulting from rubbing have adverse effects on device performance and lifetime.[1−3] Photoalignment is a noncontact method intended to avoid the problems confronting rubbing. Photoalignment also lends itself to patterning, which is instrumental to accomplishing wide viewing angles in liquid crystal displays[4] and tunability in electrooptic devices.[5−7] Three distinct approaches to photoalignment have been explored in recent years: anisotropic degradation of polyimides,[8−12] cis−trans isomerization of azobenzenes,[13−19] and anisotropic (2 + 2) cycloaddition of cinnamates[20−28] or coumarins.[4,28−36] Coumarin-containing polymers are advantageous in terms of thermal and photochemical stability without complication from isomerization in addition to offering a wide range of pretilt angle.[4] For the preparation of a photoalignment layer, a coumarin-containing polymer is normally spin-cast into a thin film in which coumarin moieties are randomly oriented. Irradiation with UV light at wavelengths longer than 300 nm causes dimerization of coumarin monomers. At a low irradiation energy (or fluence) of linearly polarized irradiation, dimerization is limited to coumarin moieties whose absorption dipoles fall along the polarization axis. These preferentially placed coumarin dimers serve to orient an overlying nematic liquid crystal along the polarization axis of UV irradiation. At a high fluence, unreacted coumarin moieties have their absorption dipoles lie largely perpendicular to the polarization axis, while coumarin dimers are nearly randomly placed. As a result, the overlying nematic liquid crystal is oriented perpendicular to the polarization axis. This crossover in liquid crystal orientation has been extensively reported in the past[29,30,35] without identifying critical parameters for a quantitative analysis.

The present study was motivated by the extent of photodimerization as a new perspective on liquid crystal orientation as illustrated by polymers containing 6- and 7-substituted coumarin pendants. Specific aims include (1) to characterize the extent of dimerization in a photoalignment film by UV−vis absorption spectroscopy, (2) to calculate the orientational order parameters for both the unreacted and reacted coumarin moieties through kinetic modeling of dimerization in a photoalignment film, (3) to characterize liquid crystal orientation on the photoalignment film as a function of the extent of dimerization, and (4) to interpret the crossover behavior in terms of the relative abundance and the orientational order of reacted and unreacted coumarin moieties in addition to the energetics of molecular interaction. To accomplish these objectives, polymers, monomers, and dimers **I** and **II** as depicted in Chart 1 were synthesized and characterized.

Experimental Section

Material Synthesis. The synthesis schemes and purification procedures for polymers, monomers, and dimers **I** and **II** are described in the Supporting Information. The analytical and ^{1}H NMR spectral data are presented in what follows.

Poly[6-[[[6-(methacryloyl)oxy]hexyl]oxy]coumarin], Polymer I. Anal. Calcd: C, 69.07; H, 6.71. Found: C, 68.89; H, 6.38. ^{1}H NMR spectral data (400 MHz, $CDCl_3$): δ 0.90−1.80 (13H, polymer main chain and spacer linkage), 3.79 (4H, −COOCH_2−, −CH_2-OAr−), 6.35 (1H, −HC═C*H*CO−, coumarin), 6.90−7.17 (3H, aromatics), 7.78 (1H, −*H*C═CHCO−, coumarin).

Poly[7-[[[6-(methacryloyl)oxy]hexyl]oxy]coumarin], Polymer II. Anal. Calcd: C, 69.07; H, 6.71. Found: C, 68.70; H, 6.74. ^{1}H NMR spectral data (400 MHz, $CDCl_3$): δ (ppm) 0.90−1.80 (13H, polymer main chain and spacer linkage), 3.96 (4H, −COOCH_2−, −CH_2OAr−), 6.19 (1H, −HC═C*H*CO−, coumarin), 6.69−6.79 (2H, aromatics), 7.32 (1H, aromatics), 7.61 (1H, −*H*C═CHCO−, coumarin).

6-(Heptyloxy)coumarin, **Monomer I.** Anal. Calcd: C, 73.82; H, 7.74. Found: C, 73.70; H, 7.80. ^{1}H NMR spectral data (400

† Department of Chemical Engineering.
‡ Laboratory for Laser Energetics.
§ Three coauthors in alphabetical order for equal contributions to this work.
* To whom correspondence should be addressed: e-mail shch@lle.rochester.edu.

10.1021/ma060269o CCC: $33.50
Published on Web 05/06/2006

Chart 1. Polymers, Monomers, and Dimers I and II Synthesized under Present Investigation

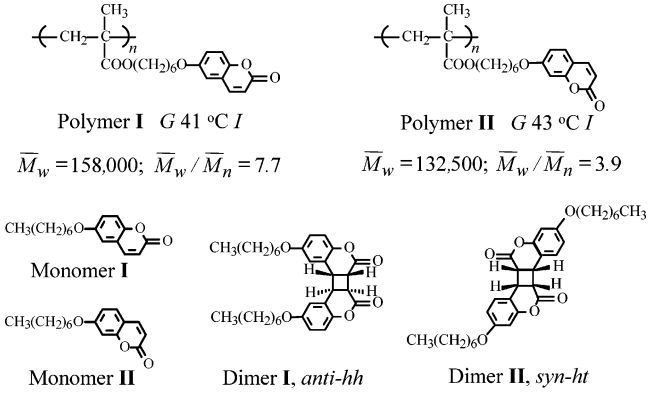

Symbols *G* for glass transition, and *I* for isotropic fluid; $\bar{M}_w$ and $\bar{M}_n$, weight- and number-average molecular weights, respectively. Regioisomerism identified as *anti-hh* and *syn-ht* following Ref. 37.

MHz, $CDCl_3$): δ (ppm) 0.88 (t, 3H, CH_3CH_2-), 1.25−1.39 (m, 6H, $CH_3CH_2CH_2CH_2CH_2-$), 1.46 (q, 2H, $-CH_2CH_2CH_2OAr-$), 1.79 (q, 2H, $-CH_2CH_2OAr-$), 3.96 (t, 2H, $-CH_2OAr-$), 6.41 (d, 1H, −HC═C*H*CO−, coumarin), 6.89 (d, 1H, aromatics), 7.10 (d, 1H, aromatics), 7.25 (d, 1H, aromatics), 7.63 (d, 1H, −*H*C═CHCO−, coumarin).

7-(Heptyloxy)coumarin, Monomer II. Anal. Calcd: C, 73.82; H, 7.74. Found: C, 73.86; H, 7.91. ^{1}H NMR spectral data (400 MHz, $CDCl_3$): δ (ppm) 0.89 (t, 3H, CH_3CH_2-), 1.25−1.39 (m, 6H, $CH_3CH_2CH_2CH_2CH_2-$), 1.46 (q, 2H, $-CH_2CH_2CH_2OAr-$), 1.80 (q, 2H, $-CH_2CH_2OAr-$), 3.98 (t, 2H, $-CH_2OAr-$), 6.23 (d, 1H, −HC═C*H*CO−, coumarin), 6.79−6.83 (m, 2H, aromatics), 7.34 (d, 1H, aromatics), 7.61 (d, 1H, −*H*C═CHCO−, coumarin).

(6aα,6bβ,12bβ,12cα)-6a,6b,12b,12c-Tetrahydro-2,11-diheptyloxycyclobuta[1,2-*c*:4,3-*c*′]dicoumarin, Dimer I. Anal. Calcd: C, 73.82; H, 7.74. Found: C, 73.61; H, 7.76. ^{1}H NMR spectral data (400 MHz, $CDCl_3$): δ (ppm) 0.89 (t, 6H, CH_3CH_2-), 1.30−1.38 (m, 12H, $CH_3CH_2CH_2CH_2$ CH_2-), 1.45 (q, 4H, $-CH_2CH_2CH_2$-OAr−), 1.76 (q, 4H, $-CH_2CH_2O$ Ar−), 3.78−3.96 (m, 8H, cyclobutane, $-CH_2OAr-$), 6.62 (d, 2H, aromatics), 6.85 (d, 2H, aromatics), 7.03 (d, 2H, aromatics).

(6aα,6bα,12aα,12bα)-6a,6b,12a,12b-Tetrahydro-3,9-diheptyloxycyclobuta[1,2-*c*:3,4-*c*′]dicoumarin, Dimer II. Anal. Calcd: C, 73. 82; H, 7.74. Found: C, 73.89; H, 7.64. ^{1}H NMR spectral data (400 MHz, $CDCl_3$): δ (ppm) 0.89 (t, 6H, CH_3CH_2-), 1.24−1.41 (m, 16H, $CH_3CH_2CH_2CH_2CH_2CH_2OAr-$), 1.70 (q, 4H, $-CH_2CH_2$-OAr−), 3.80 (m, 4H, $-CH_2OAr-$), 4.12 (m, 2H, cyclobutane), 4.24 (m, 2H, cyclobutane), 6.17 (d, 2H, aromatics), 6.64 (d, 2H, aromatics), 6.99 (d, 2H, aromatics).

Transition Temperatures and Polymer Molecular Weights. Thermal transition temperatures of polymers **I** and **II** were determined by differential scanning calorimetry, DSC (Perkin-Elmer DSC-7), with a continuous N_2 purge at 20 mL/min. Samples were preheated to 200 °C followed by cooling to −30 °C before taking the reported heating and cooling scans at 20 °C/min. The nature of phase transitions was characterized with a polarizing optical microscope (DMLM, Leica, FP90 central processor) coupled with a hot stage (FP82, Mettler Toledo). Molecular weights of polymers were determined by a size-exclusion chromatograph (model 2695 separations module, a 2487 spectrophotometric detector, and a 410 differential refractive index detector, all from Waters Corp., Milford, MA, and a model 110 differential viscometry detector, Viscotek, Porter, TX) in *N*,*N*-dimethylformamide containing 0.01 M lithium nitrate at 35 °C based on a universal calibration curve established with poly(methyl methacrylate) standards (Polymer Laboratories, Church Stretton, UK).

Film Preparation and Characterization. Polymers **I** and **II** as photoalignment films were spin-cast at 4000 rpm from 0.1 wt % chloroform solutions on optically flat fused silica substrates transparent to 200 nm (Escoproducts). For UV−vis measurements, approximately 10 and 25 nm thick films were spin-cast at 4000 rpm from 0.1 and 0.3 wt % chloroform solutions, respectively, on calcium fluoride substrates (Rubicon Technology, Inc.). Modeled as isotropic media, the spin-cast films were characterized with variable angle spectroscopic ellipsometry (V-VASE, J.A. Woollam Corp.) in terms of refractive index and thickness. The photostability of irradiated films was also investigated with FTIR spectroscopy (Brüker IFS/66 spectrometer).

Photodimerization of Polymer Films. Irradiation of polymers **I** and **II** films was performed at 90 °C under argon with a 500 W Hg−Xe lamp equipped with a filter (Oriel) that cuts wavelengths below 300 nm. Linear polarization was accomplished by a polarizing beam splitter (HPB-308 nm, Lambda Research Optics, Inc.). The irradiation intensity was monitored by a UVX digital radiometer coupled with a UVX-31 sensor (UVP, Inc.). The extent of dimerization was characterized by monitoring the UV−vis absorbance (Hewlett-Packard 8453E) of coumarin monomers in the spectral region where dimers are transparent. The direct proportionality between UV−vis absorbance and the coumarin content was established using mixtures of polymers **I** and **II** with poly(methyl methacrylate), PMMA (Polysciences, Inc., $\bar{M}_w$ = 75 000 g/mol). Insolubility of irradiated films was determined by UV−vis absorption spectroscopy after soaking in chloroform for 2 min. Irradiation at room temperature would have required a much higher fluence level to reach film insolubility.

Photoalignment of Liquid Crystal. For the characterization of their ability to orient a nematic liquid crystal, irradiated films of polymers **I** and **II** on fused silica substrates were used to prepare 10 μm thick sandwiched cells. Commercially available nematic liquid crystal, E7 (Merck) containing 0.3 wt % probing dye, M-137 (Mitsui Toatsu Dyes, Ltd.), was injected into the cell gap in the isotropic state (at 65 °C) to avoid flow-induced alignment. After thermal annealing at 55 °C for $^1/_2$ h, the cells were cooled at 10 °C/h to room temperature. For a comparative study, 10 μm thick liquid crystals were also prepared on rubbed polyimide alignment films. A UV−vis−NIR spectrophotometer (Lambda-900, Perkin-Elmer) equipped with a linear polarizer (HNP'B, Polaroid) was used to measure the orientational order parameter. Fresnel reflections from the air−glass interfaces were accounted for using a reference cell comprising an index-matching fluid sandwiched between two alignment-treated substrates.

Results and Discussion

To illustrate the crossover behavior in liquid crystal orientation, coumarin-containing polymers **I** and **II** depicted in Chart 1 were synthesized and characterized. The accompanying glass transition temperatures and molecular weights were determined by differential scanning calorimetry and size exclusion chromatography, respectively. Monomers and dimers **I** and **II**, included in Chart 1, were also synthesized and characterized to permit the extent of dimerization in photoirradiated polymer films to be monitored by UV−vis absorption spectroscopy. The regioisomerism of the resultant photodimers was positively identified on the basis of proton-NMR signals associated with the cyclobutane ring.[37] The UV−vis absorption spectra of ∼100 nm thick PMMA films containing monomer **I**, monomer **II**, and dimers **I** and **II** at mole fractions of 0.10, 0.20, and 0.33, respectively, without encountering phase separation detected as crystalline domains of the dopants, are shown in Figure 1 in terms of the extinction coefficient, $\epsilon = A/lC$, where *A*, *l*, and *C* are absorbance, film thickness, and the chromophore concentration in mole fraction, respectively. The mole fraction was calculated on the basis of the unreacted or reacted coumarin moieties and the methacrylate repeat units. The high doping levels were beneficial to an accurate measurement of ϵ in relatively thin films while ensuring a close simulation of the molecular environment in nominally concentrated films of polymers **I** and **II**. A comparison of part a with part b of

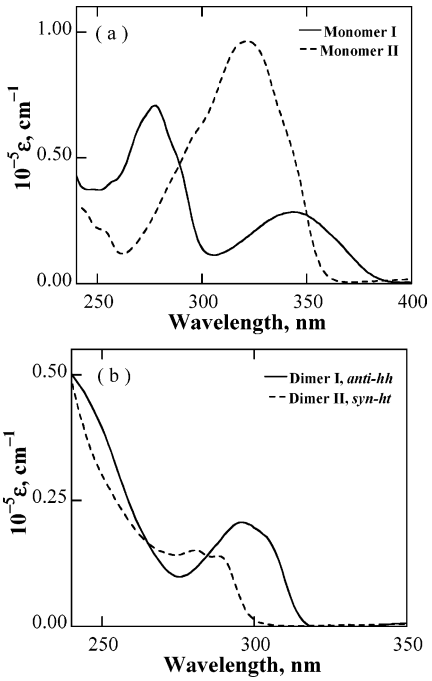

Figure 1. Extinction coefficients measured for 100 nm thick PMMA films doped with monomer **I**, monomer **II**, and dimers **I** and **II** at mole fractions of 0.10, 0.20, and 0.33, respectively.

Figure 1 reveals that the extent of monomer conversion can be determined by monitoring monomer's absorbance beyond dimer's absorption cutoff. For each type of coumarin monomer in polymers **I** and **II**, four possible regioisomers may result from photodimerization, but their absorption spectra are not expected to undergo an appreciable shift from each other, as evidenced by 6-methylcoumarin.[37]

Shown in Figure 2 are the UV−vis absorption spectra as functions of fluence for approximately 25 nm thick spin-cast films of polymers **I** and **II** on calcium fluoride substrates. The pristine films of polymers **I** and **II** yielded absorption spectra with about a 5 nm red-shift from those of monomers **I** and **II** doped in PMMA films, as the spectra in Figure 2 are compared to those in Figure 1a. The presence of isosbestic points with irradiation up to 20 J/cm^2 is an indication of stability against photodegradation, which is further substantiated by FTIR spectroscopy in the Supporting Information.

The extent of monomer conversion, X, was calculated using the UV−vis absorbances at peak maxima in the neighborhoods of 350 and 325 nm for polymers **I** and **II**, respectively. With an extinction coefficient of monomer **I** at 350 nm less than one-third that of monomer **II** at 325 nm, thicker films of polymer **I** than polymer **II** were used to ensure accuracy of the X values calculated with absorbances. Table 1 includes the calculated X values for a 24 nm thick film of polymer **I** and 10 and 27 nm thick films of polymer **II**. Film thickness, however, was found to have an insignificant effect on X for the same fluence, as demonstrated in Table 1 with a 27 nm thick film of polymer **II**. A dichroic dye, M-137, was employed to track the nematic director of a commercially available liquid crystal fluid, E-7, on the basis that the dye molecule's transition dipole is parallel to the liquid crystal's long molecular axis as demonstrated by liquid crystal orientation on uniaxially rubbed polyimide films. With 0.3 wt % of M-137 in E-7, 10 μm thick liquid crystal cells were prepared between fused silica substrates, both coated with photoalignment films that had been irradiated to a varying fluence.

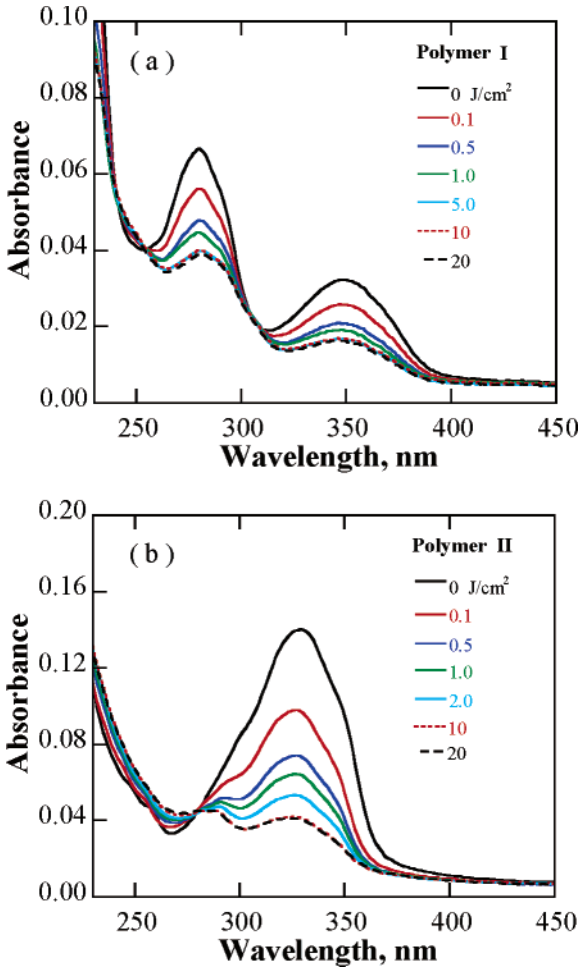

Figure 2. UV−vis absorption spectra as functions of fluence for (a) 24 nm thick polymer **I** film and (b) 27 nm thick polymer **II** film.

Table 1. Mole Fraction of Coumarin Moieties That Have Dimerized, X, and Liquid Crystal Orientational Order Parameter, S_{lc}, as Functions of Fluence[a]

	polymer **I**[b]		polymer **II**[c]		
film thickness	24 nm		27 nm	10 nm	
fluence, J/cm^2	X	S_{lc}	X	X	S_{lc}
0.1	0.23	∥ 0.74	0.38	0.37	∥ 0.71
0.2	0.31	∥ 0.75	0.43	0.40	
0.5	0.40	∥ 0.73	0.52	0.49	∥ 0.70
1.0	0.47	∥ 0.72	0.60	0.60	∥ 0.72
2.0			0.67	0.67	⊥ 0.72
5.0	0.56	∥ 0.72	0.74	0.73	⊥ 0.75
10.0	0.57	∥ 0.75	0.76	0.75	
20.0	0.57	∥ 0.78	0.76	0.75	⊥ 0.74

[a] Polarized irradiation with 4.8 mW/cm^2 at 90 °C; presented values for X and S_{lc} both accompanied by an uncertainty ±0.02; symbols ∥ and ⊥ in front of S_{lc} represent a nematic director parallel and perpendicular to the polarization axis of UV irradiation, respectively. [b] Film insolubility achieved at 0.5 J/cm^2. [c] Film insolubility achieved at 0.05 J/cm^2.

The UV−vis absorption dichroism at 643 nm served to determine the liquid crystal's orientational order parameter, $S_{lc} = (R - 1)/(R + 2)$, in which the dichroic ratio R represents the absorbance parallel divided by that perpendicular to the dye molecule's absorption dipole. The calculated S_{lc} values are prefixed by ∥ and ⊥ for a parallel and a perpendicular orientation, respectively, of the nematic director to the polarization axis of irradiation. For both polymers **I** and **II**, the photoalignment film thickness had no effect on the observed S_{lc} values. It is encouraging to note that the S_{lc} values presented in Table 1 on

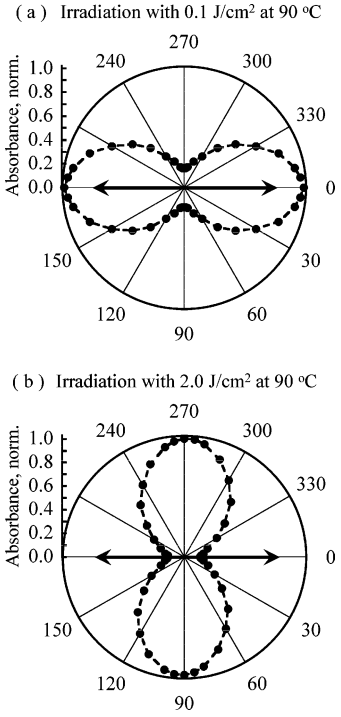

Figure 3. Polarized absorbance (at 643 nm) profiles for M-137 on 10 nm thick polymer **II** films irradiated at 90 °C with (a) 0.1 and (b) 2.0 J/cm^2 to illustrate crossover.

photoaligment films are as good as those on conventional rubbed polyimide films within an experimental error of ±0.02. The fluence levels required to achieve film insolubility in chloroform were determined to be 0.5 and 0.05 J/cm^2 for polymer films **I** and **II**, respectively. There are two reasons for polymer **II** to demand a lower fluence to reach film insolubility than polymer **I**. The 7-substituted coumarin monomer has a higher extinction coefficient for the UV irradiation than the 6-substituted coumarin monomer. In addition, the 7-substituted coumarin dimer is transparent to the irradiation, which is not the case for the 6-substituted coumarin dimer. Of particular interest is the difference in the crossover behavior between polymers **I** and **II**. With respect to the polarization axis identified by an arrow in Figure 3, a parallel and a perpendicular orientation of liquid crystal were observed on polymer **II** films at a fluence of 0.1 and 2.0 J/cm^2, respectively.

In contrast, the parallel orientation on polymer **I** persisted up to a fluence of 20 J/cm^2. It is apparent that fluence has no direct bearing on the crossover behavior. Instead, X seems to be the key parameter controlling liquid crystal orientation. A kinetic model is constructed in what follows to describe the evolutions of the mole fractions of unreacted, X_m, and reacted, X_d, coumarin moieties and their orientational order parameters, S_m and S_d.

Initially, monomeric coumarin pendants to a polymethacrylate backbone are randomly oriented in the film, as evidenced by the ellipsometric characterization of pristine films in terms of isotropic refractive indices, n, displayed in Figure 4. The random distribution of coumarin monomers can be represented as a solid sphere with a uniform density. The polarization axis of UV irradiation serves as the common reference for the treatment of photodimerization kinetics, the calculation of the order parameters pertaining to unreacted and reacted coumarin moieties, and for the characterization of liquid crystal orientation on photoirradiated films. This is equivalent to assuming that coumarin moieties' absorption dipoles are largely parallel to

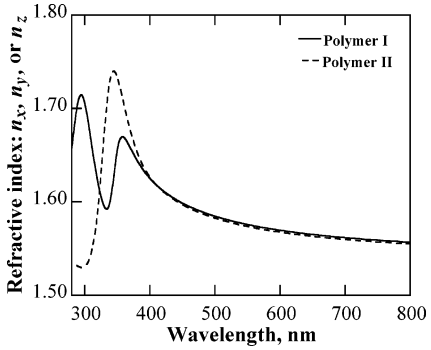

Figure 4. Isotropic refractive indices $n_x = n_y = n_z$ characterized by ellipsometry for 25 nm thick films of polymers **I** and **II**.

their molecular axes, which is supported by the measured UV−vis absorption dichroism of irradiated films. In essence, the polarization axis of irradiation plays the same role as the direction of rubbing a polyimide film in the way of defining liquid crystal orientation.

The intensity of UV irradiation absorbed by coumarin monomers is proportional to $\cos^2\theta$, where θ is the angle between a coumarin monomer's absorption dipole and the polarization axis of irradiation. As a result, the dipole moments as well as the molecular axes of both the depleting monomers and the emerging dimers are axisymmetrically distributed around the polarization axis at any time $t > 0$. The photodimerization rate of coumarin can be described by eq 1:

$$\frac{dX_d}{dt} = -\frac{dX_m}{dt} = k\exp(-t/\tau)X_m\cos^2\theta \qquad (1)$$

in which k includes the UV light intensity absorbed and the quantum yield of dimerization. This equation is intended for the surface region, where the irradiation intensity remains essentially constant and the coumarin moieties are randomly distributed to begin with. The rate of dimerization is determined by the first-order photoexcitation[38] of coumarin, and the factor $\exp(-t/\tau)$ is included to account for an exponentially decaying reaction rate with a time constant τ because of the increasing barrier to dimerization as the reaction proceeds.[39] Nevertheless, the dynamics of rotational relaxation involving coumarin monomers and dimers is not explicitly accounted for in this study.

With the initial condition $X_m = 1$, X_m and X_d are expressed as eq 2:

$$1 - X_d(\theta,t) = X_m(\theta,t) = \exp[-A(t)\cos^2\theta] \qquad (2)$$

in which $A(t) = k\tau[1 - \exp(-t/\tau)]$. Furthermore, $X(t)$ can be evaluated as follows:

$$X(t) = \frac{\int_0^\pi X_d(\theta,t)\sin\theta\, d\theta}{\int_0^\pi \sin\theta\, d\theta} = 1 - \sqrt{\frac{\pi}{4A(t)}}\,\mathrm{erf}[\sqrt{A(t)}] \qquad (3)$$

The monomer conversion data presented in Table 1 were fitted to eq 3 to arrive at $k = 0.0352\ s^{-1}$ and $\tau = 110$ s for the 24 nm thick polymer **I** film and $k = 0.0538\ s^{-1}$ and $\tau = 182$ s for the 10 nm thick polymer **II** film. The quality of curve fitting is conveyed in Figure 5, which also reveals the failure of simple first- and second-order reactions without $\exp(-t/\tau)$[40,41] to capture the asymptotic behavior in X.

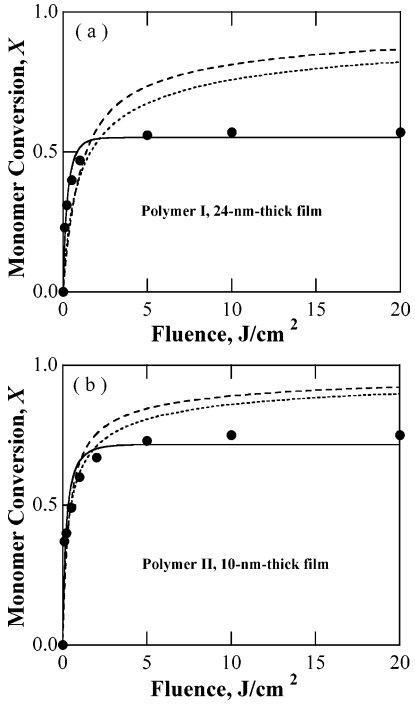

Figure 5. Monomer conversion as a function of fluence at 90 °C: (a) 24 nm thick polymer **I** film and (b) 10 nm thick polymer **II** film. Filled circles for experimental data; solid, dashed, and dotted curves representing respectively the best fit to eq 3, first-order reaction, $X(t) = 1 - \sqrt{\pi/4kt}\ \mathrm{erf}(\sqrt{kt})$ with $k = 0.0108$ and $0.0312\ \mathrm{s}^{-1}$ for polymers **I** and **II**, and second-order reaction, $X(t) = 1 - \tan^{-1}(\sqrt{kt})/\sqrt{kt}$ with $k = 0.0160$ and $0.0532\ \mathrm{s}^{-1}$ for polymers **I** and **II**.

With the established rate expression for photodimerization, let us proceed to evaluate the ensemble average of $\cos^2\theta$ using eq 4:

$$\langle \cos^2\theta \rangle (t) = \frac{\int_0^\pi f(\theta,t) \cos^2\theta \sin\theta \, \mathrm{d}\theta}{\int_0^\pi f(\theta,t) \sin\theta \, \mathrm{d}\theta} \tag{4}$$

in which the orientational distribution function $f(\theta,t) = X_\mathrm{m}(\theta,t)$ or $X_\mathrm{d}(\theta,t)$. The resultant $\langle \cos^2\theta \rangle_\mathrm{m}$ and $\langle \cos^2\theta \rangle_\mathrm{d}$ are subsequently entered into the general expression of the orientational order parameter, $S = (3\langle \cos^2\theta \rangle - 1)/2$, to arrive at $S_\mathrm{m}(t)$ and $S_\mathrm{d}(t)$ as follows:

$$S_\mathrm{m}(t) = \frac{3}{4A(t)} - \frac{1}{2} - \frac{3\exp[-A(t)]}{2\sqrt{\pi A(t)}\ \mathrm{erf}[\sqrt{A(t)}]} \tag{5}$$

$$S_\mathrm{d}(t) = \frac{[3 - 2A(t)]\sqrt{\pi}\ \mathrm{erf}[\sqrt{A(t)}] - 6\sqrt{A(t)}\exp[-A(t)]}{4A(t)\{\sqrt{\pi}\ \mathrm{erf}[\sqrt{A(t)}] - 2\sqrt{A(t)}\}} \tag{6}$$

Finally, S_m and S_d can be established as functions of X through the relationship between X and A in eq 3. For both $S_\mathrm{m}(X)$ and $S_\mathrm{d}(X)$, the polarization axis of irradiation serves as the optic axis, viz. the direction in which light propagates without experiencing optical birefringence, because of the axisymmetric dimerization process.

Equation 4 together with the general expression of S yields two limiting cases: $S_\mathrm{m} \to 0$ and $S_\mathrm{d} \to 0.4$ as $X \to 0$. Furthermore, it is noted that as $t \to \infty$, $A(t) \to k\tau$ and hence $X \to 1 - \sqrt{\pi/4k\tau}\ \mathrm{erf}(\sqrt{k\tau})$, suggesting a monotonic increase in X with an increasing $k\tau$. The complete solutions for S_m and S_d as functions of X are plotted in Figure 6 for the case of $\tau \to \infty$, in which the

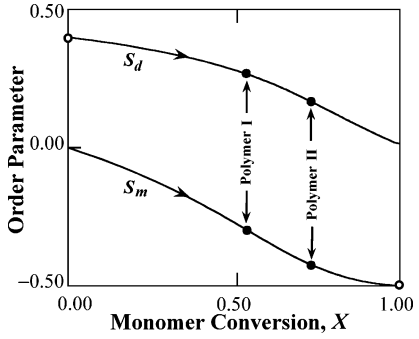

Figure 6. Orientational order parameter, S_m and S_d, calculated for polymer **I** and **II** films as functions of monomer conversion X. Symbols: open circles for discontinuity and filled circles for termini of photodimerization.

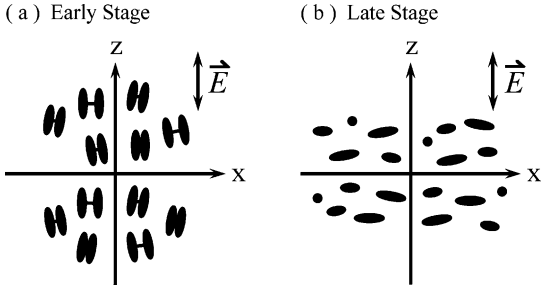

Figure 7. Orientation of the motivating species in a photoalignment film: (a) coumarin dimers at the early stage of dimerization; (b) coumarin monomers at the late stage of dimerization, with $\vec{E}$ representing the electric field of polarized irradiation.

open circles denote discontinuity as dimers do not exist at $X = 0$ and neither do monomers at $X = 1$.

Since S_m and S_d are expressed in eqs 5 and 6 as functions of A, which is related to X via eq 3, the profiles shown in Figure 6 are applicable to any combination of k and τ that contributes to X. The filled circles identify where dimerization ends, $X(t \to \infty) = 0.55$ and 0.72 for polymers **I** and **II**, respectively, with finite τ values. The good agreement between the calculated terminal monomer conversions and the observed asymptotic X values is another evidence for the excellent quality of curve fitting.

According to eqs 5 and 6, $S_\mathrm{d} \to 0$ and $S_\mathrm{m} \to -0.5$ in the limit of $X \to 1$, namely, both $k\tau$ and $t \to \infty$. Note that the algebraic signs of S_d and S_m indicate that the reacted and unreacted coumarin moieties are oriented parallel and perpendicular to the polarization axis, respectively. The modeling results enable the visualization of coumarin dimers and monomers that are responsible for orientating liquid crystals. At the early stage of dimerization, the reacted coumarin moieties' absorption dipoles are distributed around the polarization (or z-) axis because of the proportionality to $\cos^2\theta$ of dimerization rate; as $X \to 0$, $S_\mathrm{d} \to 0.4$ rather than 1. Figure 7a depicts the reacted coumarin moieties on the x,z-plane parallel to the film surface, on which liquid crystal molecules organize themselves along the z-axis.

At the late stage of dimerization, the unreacted coumarin moieties approach a random orientation on the x,y-plane. On the x,z-plane, however, a fraction of unreacted coumarin moieties are oriented along the x-axis, as depicted in Figure 7b, which is characterized by $|S_\mathrm{m}|$ close to its limiting value of 0.5. The orientational order parameter would be unity if all the unreacted coumarin moieties were oriented parallel to the x-axis. Apparently, a limited extent of orientation on the part of the unreacted coumarin moieties with their axes parallel to the x-axis is sufficient to cause crossover if dimerization is allowed to

proceed to an advanced stage. Both the relative abundance of the two coumarin moieties and the degrees of their respective orientation will serve as a foundation for the discussion of crossover in liquid crystal orientation in what follows.

The results presented in Table 1 indicate that liquid crystal orientation on polymer **II** undergoes a crossover at $X = 0.67$ but not on polymer **I** up to $X = 0.57$. The orientation of a liquid crystal with reacted vs unreacted coumarin moieties had been investigated in terms of molecular interaction of dispersive and steric origins. The main conclusion was that the unreacted coumarin moieties are more planar with more extended π-conjugation, thus interacting more strongly with an overlying liquid crystal than the reacted moieties.[29,30] In addition to the energetics of molecular interaction, both the relative abundance and the degree of orientational order are quantified for explaining crossover. The reacted and unreacted coumarin moieties dominate liquid crystal orientation at a low and high conversion, respectively. This general observation suggests that the relatively high orientational order parameters of the two motivating species, $S_d \rightarrow 0.4$ and $|S_m| \rightarrow 0.5$, play predominant roles. At the intermediate stage where crossover is likely to happen, the relative abundance of the two seems to be a competing factor. Two possible scenarios are considered: the unreacted and reacted coumarin moieties competing for liquid crystal orientation on a 1-to-1 and 1-to-2 basis.

In the 1-to-1 scenario for polymer **I**, the reacted coumarin moieties dominate liquid crystal orientation up to $X = 0.57$ presumably because of the higher abundance of reacted than unreacted coumarin moieties (57:43) despite the marginally inferior order, $S_d = 0.24$ vs $|S_m| = 0.33$ (see Figure 6), and less favorable energetics. In the case of polymer **II**, crossover occurred at $X = 0.67$, suggesting that unreacted coumarin moieties take over from reacted moieties because of the better orientational order, $|S_m| = 0.40$ vs $S_d = 0.19$ (see Figure 6), and more favorable energetics despite the numerical inferiority, 33:67. The 1-to-2 scenario is equivalent to a coumarin dimer competing with an unreacted coumarin monomer for liquid crystal orientation. At $X = 0.57$ in polymer **I**, unreacted moieties are in favor in terms of orientational order, $|S_m| = 0.33$ vs $S_d = 0.24$, relative abundance, 43:29, and favorable energetics. On all three accounts, crossover should have taken place, which is at odds with experiment. As for polymer **II** at $X = 0.67$, the two orienting species are nearly balanced in abundance, 33:34, but both the orientational order, $|S_m| = 0.40$ vs $S_d = 0.19$, and energetics are in favor of crossover, consistent with the experimental observation. Overall, the 1-to-1 scenario seems to delineate a more convincing physical picture than the 1-to-2 scenario. This interpretation reveals the intricate roles played by the relative abundance and orientational order of the two orthogonal motivating species in liquid crystal orientation.

Conclusions

Polymers **I** and **II** containing 6- and 7-substituted coumarin moieties, respectively, were spin-cast into thin films for a systematic investigation of liquid crystal orientation. The initially isotropic films were irradiated with linearly polarized UV light to a varying fluence, resulting in photoalignment films whose ability to orient a nematic liquid crystal, E-7, was assessed in terms of the orientation order parameter, S_{lc}, of a dichroic dye, M-137. It is encouraging to note that the S_{lc} values achieved on films of polymers **I** and **II** are comparable to that on uniaxially rubbed polyimide films. Monomers and dimers **I** and **II** were synthesized for the characterization of UV−vis absorption spectra to furnish new insight into photoalignment of liquid crystals from the standpoint of monomer conversion, X. To identify the factors responsible for the crossover in liquid crystal orientation on photoalignment films, a kinetic model was constructed to describe the unreacted and reacted coumarin moieties' orientational order parameters, S_m and S_d, as functions of X. Key findings are recapitulated as follows:

(1) Liquid crystal orientation on the polymer **I** film remained parallel to the polarization axis up to a fluence of 20 J/cm^2 primarily because of X limited to 0.57 by a relatively low absorbance of UV irradiation on the part of monomer **I** with which dimer **I** competes for irradiation energy.

(2) In contrast, a transition from a parallel to a perpendicular orientation was observed on the polymer **II** film at a fluence of 2.0 J/cm^2 corresponding to $X = 0.67$. Because of a relatively high absorbance of UV irradiation on the part of monomer **II** with which dimer **II** does not compete for irradiation energy, the polymer **II** film proceeded to a higher asymptotic X value than the polymer **I** film, 0.75 vs 0.57.

(3) A mathematical model of photodimerization was constructed on the basis of first-order kinetics involving an exponentially decaying rate constant to account for an increasing barrier as the reaction proceeds. Successfully validated with the experimental data for X as a function of irradiation time, the kinetic model is instrumental to delineating how coumarin dimers and monomers orient liquid crystals at the early and the late stages of photodimerization, respectively.

(4) The kinetic model was used to predict S_m and S_d as functions of X for an interpretation of crossover in liquid crystal orientation based on the relative abundance and the degree of orientational order governing the two motivating species, unreacted and reacted coumarin moieties existing in monomer and dimer **II**, in addition to the energetics of molecular interaction. Of the two scenarios under consideration, the one in which unreacted and reacted coumarin moieties compete for liquid crystal orientation on a 1-to-1 basis appears to delineate a more convincing physical picture than 1-to-2.

Acknowledgment. The authors thank Dr. Thomas H. Mourey of Eastman Kodak Company for the characterization of the molecular weight distributions of polymers **I** and **II** by size exclusion chromatography and Dr. Jane J. Ou of Chemical Engineering Department at the University of Rochester for helpful discussions regarding computational chemistry and kinetic modeling. They are grateful for the financial support provided by the Eastman Kodak Company, the New York State Center for Electronic Imaging Systems, and the National Science Foundation under Grant CTS-0204827. Additional funding was provided by the Department of Energy Office of Inertial Confinement Fusion under Cooperative Agreement No. DE-FC03-92SF19460 with the Laboratory for Laser Energetics and the New York State Energy Research and Development Authority. The support of DOE does not constitute an endorsement by DOE of the views expressed in this article.

Supporting Information Available: Synthesis and purification of monomers, dimers, and polymers **I** and **II**, regioisomerism of dimers I and II by ^{1}H NMR spectra, and FTIR spectra of the spin-cast films of polymers **I** and **II** as well as PMMA films containing monomers and dimers **I** and **II**. This material is available free of charge via the Internet at http://pubs.acs.org.

References and Notes

(1) Toney, M. F.; Russell, T. P.; Logan, J. A.; Kikuchi, H.; Sands, J. M.; Kumar, S. K. *Nature (London)* **1995**, *374*, 709−711.

(2) (a) Sakamoto, K.; Arafune, R.; Ito, N.; Ushioda, S.; Suziki, Y.; Morokawa, S. *J. Appl. Phys.* **1996**, *80*, 431−439. (b) Stöhr, M.; Samant, M. G.; Cossy-Favre, A.; Diaz, J.; Momoi, Y.; Odahara, S.; Nagata, T. *Macromolecules* **1998**, *31*, 1942−1946.
(3) (a) Ishihara, S. *IEEE/OSA J. Display Technol.* **2005**, *1*, 30−40. (b) Bechtold, I. H.; De Santo, M. P.; Bonvent, J. J.; Oliveira, E. A.; Barberi, R.; Rasing, T. *Liq. Cryst.* **2003**, *30*, 591−598.
(4) (a) Schadt, M.; Seiberle, H.; Schuster, A. *Nature (London)* **1996**, *381*, 212−215. (b) Schadt, M.; Seiberle, H. *JSID* **1997**, *5*, 367−370.
(5) Gupta, V. K.; Abbott, N. L. *Science* **1997**, *276*, 1533−1536.
(6) Patel, J. J.; Rastani, K. *Opt. Lett.* **1991**, *16*, 532−534.
(7) Chen. J.; Bos, P. J.; Vithana, H.; Johnson, D. L. *Appl. Phys. Lett.* **1995**, *67*, 2588−2590.
(8) Hasegawa, M.; Taira, Y. *J. Photopolym. Sci. Technol.* **1995**, *8*, 241−248.
(9) Gong, S.; Kanicki, J.; Ma, L.; Zhong, J. Z. Z. *Jpn. J. Appl. Phys.* **1999**, *38*, 5996−6004.
(10) Lu, J.; Deshpande, S. V.; Gulari, E.; Kanicki, J.; Warren, W. L. *J. Appl. Phys.* **1996**, *80*, 5028−5034.
(11) Sung, S.-J.; Lee, J.-W.; Kim, H.-T.; Park, J.-K. *Liq. Cryst.* **2002**, *29*, 243−250.
(12) (a) Xu, C.; Shiono, T.; Ikeda, T.; Wang, Y.; Takeuchi, Y. *J. Mater. Chem.* **2003**, *13*, 669−671. (b) Zhong, Z.-X.; Li, X.; Lee, S. H.; Lee, M.-H. *Appl. Phys. Lett.* **2004**, *85*, 2520−2522.
(13) Gibbons, W. M.; Shannon, P. J.; Sun, S.-T.; Swetlin, B. J. *Nature (London)* **1991**, *351*, 49−50.
(14) Shannon, P. J.; Gibbons, W. M.; Sun, S.-T. *Nature (London)* **1994**, *368*, 532−533.
(15) Ichimura, K.; Suzuki, Y.; Seki, T.; Hosoki, A.; Aoki, K. *Langmuir* **1988**, *4*, 1214−1216.
(16) Ichimura, K. *Chem. Rev.* **2000**, *100*, 1847−1874.
(17) Ikeda, T. *J. Mater. Chem.* **2003**, *13*, 2037−2057.
(18) Furumi, S.; Kidowaki, M.; Ogawa, M.; Nishimura, Y.; Ichimura, K. *J. Phys. Chem. B* **2005**, *109*, 9245−9254.
(19) Sévigny, S.; Bouchard, L.; Montallebi, S.; Zhao, Y. *Liq. Cryst.* **2005**, *32*, 599−607.
(20) Schadt, M.; Schmitt, K.; Kozinkov, V.; Chigrinov, V. *Jpn. J. Appl. Phys.* **1992**, *31*, 2155−2164.
(21) Schadt, M.; Seiberle, H.; Schuster, A.; Kelly, S. M. *Jpn. J. Appl. Phys.* **1995**, *34*, L764−L767.
(22) Cull, B.; Shi, Y.; Kumar, S.; Schadt, M. *Phys. Rev. E* **1996**, *53*, 3777−3781.
(23) Obi, M.; Morino, S.; Ichimura, K. *Jpn. J. Appl. Phys.* **1999**, *38*, L145-L147.
(24) Kawatsuki, N.; Ono, H.; Takatsuka, H.; Yamamoto, T.; Sangen, O. *Macromolecules* **1997**, *30*, 6680−6682.
(25) (a) Kawatsuki, N.; Matsuyoshi, K.; Hayashi, M.; Takatsuka, H.; Yamamoto, T. *Chem. Mater.* **2000**, *12*, 1549−1555. (b) Kawatsuki, N.; Takatsuka, H.; Yamamoto, T.; Ono, H. *Jpn. J. Appl. Phys.* **1997**, *36*, 6464−6469.
(26) Ichimura, K.; Akita, Y.; Akiyama, H.; Kudo, K.; Hayashi, Y. *Macromolecules* **1997**, *30*, 903−911.
(27) Stump, A.; Gubler, U.; Bosshard, C. *Opt. Lett.* **2005**, *30*, 1333−1335.
(28) Perny, S.; Barny, P. L.; Delaire, J.; Buffeteau, T.; Sourisseau, C.; Dozov, I.; Forget, S.; Martinot-Lagarde, P. *Liq. Cryst.* **2000**, *27*, 329−340.
(29) Obi, M.; Morino, S.; Ichimura, K. *Chem. Mater.* **1999**, *11*, 656−664.
(30) Jackson, P. O.; O'Neill, M.; Duffy, W. L.; Hindmarsh, P.; Kelly, S. M.; Owen, G. J. *Chem. Mater.* **2001**, *13*, 694−703.
(31) Kawatsuki, N.; Goto, K.; Yamamoto, T. *Liq. Cryst.* **2001**, *28*, 1171−1176.
(32) (a) Contoret, A. E. A.; Farrar, S. R.; Jackson, P. O.; Khan, S. M.; May, L.; O'Neill, M.; Nicholls, J. E.; Kelly, S. M.; Richards, G. J. *Adv. Mater.* **2000**, *12*, 971−974. (b) Lee, J.; Lee, J.-I.; Sung, S.-J.; Chu, H. Y.; Park, J.-K.; Shim, H.-K. *Macromol. Chem. Phys.* **2004**, *205*, 2245−2251.
(33) Tian, Y.; Akiyama, E.; Nagase, Y. *J. Mater. Chem.* **2003**, *13*, 1253−1258.
(34) Trenor, S. R.; Shultz, A. R.; Love, B. J.; Long, T. E. *Chem. Rev.* **2004**, *104*, 3059−3077.
(35) O'Neill, M.; Kelly, S. M. *J. Phys. D: Appl. Phys.* **2000**, *33*, R67−R84.
(36) Aldred, M. P.; Contoret, A. E. A.; Farrar, S. R.; Kelly, S. M.; Mathieson, D.; O'Neill, M. O.; Tsoi, W. C.; Vlachos, P. *Adv. Mater.* **2005**, *17*, 1368−1372.
(37) Yu, X.; Scheller, D.; Rademacher, O.; Wolff, T. *J. Org. Chem.* **2003**, *68*, 7386−7399.
(38) Kopecký, J. *Organic Photochemistry: A Visual Approach*; VCH Publishers: New York, 1992; p 44.
(39) Ionescu, A. T.; Barberi, R.; Giocondo, M.; Iovane, M.; Alexe-Ionescu, A. L. *Phys. Rev. E* **1998**, *58*, 1967−1972.
(40) Chen, Y.; Wu, J.-D. *J. Polym. Sci., Part A: Polym. Chem.* **1994**, *32*, 1867−1875.
(41) Azuma, C.; Sanui, K.; Ogata, N. *J. Appl. Polym. Sci.* **1982**, *27*, 2065−2078.

MA060269O